1992

Modeling and Simulation of a Scroll Compressor Using Bond Graphs

D. L. Margolis
University of California

S. Craig
University of California

G. Nowakowski
Gas Research Institute

M. Inada
Aisin Seiki Company

M. Dearing
Aisin Seiki Company

MODELING AND SIMULATION OF A SCROLL COMPRESSOR USING BOND GRAPHS

by

Donald L. Margolis
Professor

Scott Craig
Research Assistant

Department of Mechanical Engineering
University of California
Davis, CA 95616

Gary Nowakowski
Gas Research Institute

and

Masami Inada
Michael Dearing
Aisin Seiki Company, Ltd.

Abstract

A model has been developed for a three chamber scroll compressor using bond graphs. Mechanical and thermodynamic bond graph elements are incorporated into the model. The model includes area modulation based on the geometry of the scroll wraps as well as the orbit angle, mass delay, flank leakage, and radial leakage. A two-phase flow model which takes into account a gas/liquid fluid mixture, typical of refrigerants was developed. A heat transfer model was also developed for energy exchange between the fluid and case. The bond graph and results from three simulations are discussed. They are the loss and leakage free case with mass delay and area modulation, flank leakage for quality equal to 100%, and two-phase flow with quality equal to 50% and 1%.

Introduction

Bond graphs have been used extensively to model all types of energetic systems [8]. They are useful in determining characteristics of systems for analysis and design purposes. Bond graphs have been used previously to model rotating machines, specifically, the screw compressor, [1], the Roots blower, [2], and the Wankel compressor, [3].

The scroll compressor has been studied extensively in recent years. In particular, modeling and simulation of the compressor with various characteristics have been carried out, and the results published (see for example Refs. [4], [5], [6], and [7]. This paper discusses the use of bond graphs to model the compressor in order to better understand the interactive dynamics and to aid in the design of these machines.

The Model

A typical scroll compressor is shown in Fig. 1, and the compression sequence shown in Fig. 2. The scroll compressor consists of a pair of scroll wraps. One scroll is fixed to the housing of the machine, while the other wrap orbits around the center of the stationary wrap at a constant radius. The wraps are identical in geometry. However, one wrap is rotated 180 degrees with respect to the other so that several contact points between the orbiting scroll and the fixed scroll exist. An Oldham coupling keeps the orbiting scroll from rotating and thereby maintain the 180 degree orientation. As the moving scroll orbits, the intake port is exposed, and fluid enters the periphery of the wraps and is trapped in crescent shaped pockets. The pockets decrease in volume, and the trapped fluid is discharged at a specified orbit angle.

Bond Graph Model

The bond graph developed to model and simulate a three chamber scroll compressor with leakage and two-phase flow is shown in Fig. 3. The elements comprising the model are the effort and flow sources (S_e and S_f), transformers (TF), modulated transformers (MTF), thermodynamic accumulators (C), isentropic nozzles (R), and the inertial elements (1). References [8] and [9] are suggested for details regarding the foregoing. Also, an Appendix is included which briefly introduces bond graph modeling. Each component of the hand graph of Fig. 3 is described next.

Mechanical Dynamics

The angular velocity, ω_i, from the drive motor is the input to the system, and is represented by the flow source (S_f) on bond 1 of Fig. 3. The transformer between bonds 1 and 2 serves as a gear reducer. The product of the TF modulus and ω_i yields the orbit angular velocity, ω_o. These are the flow variables on bonds 3, 17, and 29. MTF's convert the orbiting angular velocity into a rate of change in chamber volume by the relationship of eqn. (1). These volume rates are the flows on bonds 4, 18, and 30. The modulus of the MTF is the slope of the volume vs orbit angle curve and changes as the scroll orbits. The dV/dt term sets the flow on the "true bond" of the accumulator, i.e., flows on bonds 7, 21, and 33, where

$$\frac{dV}{dt} = \left(\frac{dV}{d\theta}\right)\left(\frac{d\theta}{dt}\right) \qquad (1)$$

The instantaneous volumes of the chambers are determined by integrating (1). Through the ideal gas law, the pressure and temperature of the chambers are calculated as discussed below and are outputs from the C-elements. The pressures of the chambers set the efforts on the 0-junctions, i.e., efforts on bonds 7, 21, and 33. The pressures of the chambers are absolute pressures. The gage pressure of each chamber, efforts on bonds 4, 20, and 30, is obtained by subtracting atmospheric pressure, i.e., efforts on bonds 5, 19, and 31, from the absolute pressure of the chamber.

The torque, T, is related to the pressure, P, by eqn. (2),

$$T\left(\frac{d\theta}{dt}\right) = P\left(\frac{dV}{dt}\right) \tag{2}$$

which is a statement of ideal power conservation. Substituting equation (1) into (2) yield,

$$T = P\left(\frac{dV}{d\theta}\right) \tag{3}$$

Thus, the gage pressure of the chamber multiplied by the modulus, $dV/d\theta$, yields the torque required to compress the fluid. These are the efforts on bonds 3, 17, and 29. The product of the sum of the torques and the modulus of the transformer (TF) yields the drive motor output torque. The input power is the product of the input angular velocity and the output torque.

Thermodynamic Model

Two thermodynamic elements are used in the model; the thermodynamic accumulator (Fig. 4) and the isentropic nozzle (Fig. 5). For complete details pertaining to the thermodynamic elements Ref. [10] is suggested.

Thermodynamic Accumulator

To account for the mass and energy entering, stored, and exhausted from the chambers, thermodynamic accumulators are used. The temperature, T, and pressure, P, of the chamber are determined through the constitutive relations (4) and (5). These equations are derived from the ideal gas laws as,

$$T = \frac{E}{C_v M} \tag{4}$$

$$P = \frac{R\ E}{C_v V} \tag{5}$$

where E is the energy in the control volume, R is the universal gas constant, C_v is specific heat at constant volume, V is the volume, M is mass of fluid, and P is the absolute pressure within the chamber. It is assumed for the purposes of modeling that the fluid mixture in the chamber is homogeneous at any time, thus a single temperature and pressure represents the properties of the fluid in the chamber.

As causality indicates in Fig. 4 (perpendicular strokes at the end of each bond), the thermodynamic accumulator receives as inputs the mass flow, $\dot{m}$, energy flow, $\dot{E}$, and volume expansion rate, $\dot{V}$. It integrates these quantities to obtain the mass, M, energy, E, and volume, V, and then delivers as outputs the temperature and pressure from eqns. (4) and (5). As long as this causality is maintained, then the equations for the accumulator can be written once, and computer coded in an automated fashion, for multiple volumes.

In order to use the accumulator, the input "flows" must be specified. This is accomplished with the isentropic nozzle described next.

Isentropic Nozzle

The isentropic nozzle serves two purposes in the model. It represents the intake and exhaust ports which govern the mass and energy flow into and out of the compression chamber (thermodynamic accumulators), and it is used to model flank and radial leakage between the chambers. Fig. 5 shows the nozzle as a 4-port R-element that receives temperature and pressure

as causal inputs, and delivers mass flow and energy flow as outputs. The constitutive law used to determine mass flow through the nozzle is given by eqn. (6),

$$\dot{m} = Ac_d \frac{Pu}{\sqrt{T_u}} \sqrt{\frac{2\gamma}{R(\gamma-1)}} \sqrt{P_r^{(2/\gamma)} - P_r^{(\frac{\gamma+1}{\gamma})}} \tag{6}$$

where A (θ) is the cross sectional area of the intake or exhaust ports which are functions of the orbit angle, θ, and the scroll wrap geometry. The quantity, γ, is the ratio of specific heats and is assumed constant in this model, i.e.,

$$\gamma = \frac{C_p}{C_v} = 1.4 \ (for\ air) \tag{7}$$

The critical pressure ratio is defined as,

$$P_{cr} = \left(\frac{2}{\gamma+1}\right)^{\left(\frac{\gamma}{\gamma-1}\right)} = 0.53 (for\ air) \tag{8}$$

and the pressure ratio is,

$$P_r = \frac{Downstream pressure}{Upstream pressure} \tag{9}$$

Since P_a and P_b are inputs to the 4-port R, the upstream pressure is selected to be whichever pressure, P_a or P_b, is larger. The 4-port R is used by computing the pressure ratio, P_r, from the input pressures. The effective pressure ratio is set to the critical pressure ratio, P_{cr}, when the pressure ratio, P_r, is less than or equal to the critical pressure ratio. The effective pressure ratio is otherwise set to the value of the calculated pressure ratio. When the pressure ratio is less than P_{cr} the flow is choked.

The mass flow, $\dot{m}$, is calculated from (6) as one of the outputs from the 4-port R-element, and energy flow is calculated from the mass flow as,

$$\dot{E} = \dot{m}h \tag{10}$$

$$= \dot{m} C_p T_u \tag{11}$$

where C_p = Specific heat at constant pressure
T_u = Upstream temperature (another input to the R-element)

The sign of the flows $\dot{m}_a$, $\dot{m}_b$, $\dot{E}_a$, $\dot{E}_b$, is determined by whichever pressure, P_a or P_b, is larger. This same computational procedure is followed for intake, exhaust and leakage flows.
The flank leakage area of the nozzle is equal to the height of the scroll wrap multiplied by the clearance existing between the orbiting and fixed scroll. The leakage area is kept constant throughout the compression cycle. The program allows the user to set the clearance to any desired value. This allows the user to study the effects of leakage on the performance of the compressor by varying the value of the clearance.

Radial leakage is dynamically identical to flank leakage, but the leakage flow area is more complicated to compute. This is discussed in a following section..

Area Modulation for the Intake and Exhaust Port, and Mass Delay

The intake and exhaust ports are governed by the following equations obtained from Tojo [5].

$$Area(\theta)_{intake} = h\zeta(1-\cos\theta) \tag{12}$$

$$Area(\theta)_{exhaust} = h\left\{r_c - \sqrt{\zeta^2-(r_c-\zeta)^2-2\zeta(r_c-\zeta)\cos(\pi-\theta)}\right\} \tag{13}$$

where h is the scroll wrap height, ζ is the crank arm radius, and r_c is the cutter radius.

The mass flow rate from eqn. (6) is instantaneously determined once the pressure ratio is prescribed. When a chamber volume is small (such as at the initiation of intake or when the exhaust opens) the instantaneous mass flow can sometimes "overcharge" the volume in a short (but not short enough) integration time interval. This shows up as a chatter phenomenon and has nothing to do with the goodness of the model. Shortening the integration step can alleviate the problem, but variable time step integration methods do not interpret this oscillation as a problem. In fact, this oscillation rarely leads to numerical instability, and usually is numerically damped as the pressure ratio across the port tends toward unity.

Keeping in mind that we do not want to interfere with the causality of the 4-port R-element, we have found that delaying the mass flow rate provides a cure for the problem. Phenomenologically, we realize that the mass flow will not instantly occur when a pressure ratio exists, because of fluid inertial effects. Rather than introduce an inertial element (which will alter the 4-port R causality), we delay the mass flow rate by the first order filter,

$$\frac{d}{dt}\dot{m} = \frac{\dot{m}_{des}-\dot{m}}{\tau} \tag{14}$$

where $\dot{m}_{des}$ is the mass flow rate from eqn. (6). The time constant, τ, is selected to be sufficiently small so that the system dynamics are not adversely effected, but large enough to prevent chatter.

Volume as a function of the Orbit Angle

The equations for the chamber volume as a function of the orbit angle were obtained from Morishita [4].

Volume of the outermost chamber

For $0 < \theta <$ angle at which compression begins

$$V_1(\theta) = (V_{max}-V_{min})2\pi \tag{15}$$

where V_{max} is the volume at $\theta \approx$ angle at which compression begins
V_{min} is the volume at $\theta =$ angle at which discharge commences

For the angle at which compression begins $<\theta<360$

$$V_1(\theta) = p\pi(p-2t)h\{(2i-\theta/\pi)\} \quad where\ i=3 \tag{16}$$

Volume of the intermediate chamber

For 360 < θ < angle at discharge (θ^*)

$$V_2(\theta) = p\pi(p-2t)h\{(2i-1)-\theta/\pi\} \quad (17)$$

Where $i=2$

For angle at discharge (θ^*) < θ < 720

$$V_2(\theta) = 1/3a^2h\{9/2\pi-\alpha-\theta)^3-(7/2\pi-\alpha-\theta)^3\}-2\alpha^2ha \quad (18)$$
$$.(7/2\pi-\theta)^2\}-2/3a^2h\alpha^3+(-S+2S')h$$

Volume of the innermost chamber

For 720 < θ < angle at which discharge begins, (θ^*)

$$V_3(\theta) = 1/3a^2h\{(5/2\pi-\alpha-\theta)^3-(3/2\pi-\alpha-\theta)^3\}-2\alpha^2ha \quad (19)$$
$$(3/2\pi-\theta)^2-2/3a^2h\alpha^3+(-S+2S')h$$

Note: S is defined in the appendix. S' is an area to be determined from the interaction between the cutter and the involute.

θ^* = Angle of discharge commencement
$V(\theta)$ = Volume of chamber as a function of the orbit angle
θ = Orbiting Angle
h = Height of scroll
a = Base circle radius
p = Pitch
t = Thickness of scroll wrap
α = Involute initial angle
N = Number of scrolls - 1/4

Flank and Radial Leakage

Tip leakage and flank leakage between the scroll wraps diminishes the compressors performance. Flank leakage between the compression chambers as shown in Fig. 6 is incorporated into the model.

Leakage communication between the chambers is accomplished through the use of the isentropic nozzle element. The leakage area is the product of the scroll wrap height and the clearance. The clearance is the distance between the fixed and orbiting scroll.

The radial leakage between scroll chambers occurs because there is not perfect sealing at the top and bottom of the scroll wraps. The leakage path is indicated in Fig. 6. The leakage area is the product of a clearance and the scroll wrap length. Computation of the wrap length is not included here. Radial leakage is included in the model, and its effect is demonstrated in some simulation results.

Two-Phase Flow

A separated two-phase flow model as shown in Fig. 7 was developed. The liquid and vapor phases are modeled as two separate bodies of fluid entering the compressor intake. The assumption is that liquid with its high density when compared with air, flows at the bottom of the suction line, while the vapor flows on top of the liquid. It is also assumed that thermal energy transferred between the vapor and liquid in the chamber is small due to the relatively short time the fluid is resident in the machine. The flow energy of the liquid is also considered to be small compared with the flow energy of the gas.

The two-phase flow model relies on the use of a 1-port inertial element; Fig. 8. The inertial bond sets the liquid volumetric flowrate into the chamber volume as shown on bonds 51, 54, and 57 in Fig. 3. The volume flow is integrated to yield the instantaneous volume of liquid that enters the compression chamber. The volume difference between the physical volume and the liquid volume is the volume of the chamber available for receiving and compressing the gas. It should be noted that if the ingested liquid volume exceeds the minimum chamber volume at exhaust, then at some time during compression the machine will hydraulically lock, and the actual device would probably structurally fail.

Liquid flow into the compression chamber is governed by the pressure difference between the compression chamber and the pressure outside the intake. This outside pressure is set to atmospheric pressure for the simulation results in this paper.

During the intake process, the volume in the compression chamber increases. The pressure in the chamber drops below atmospheric pressure, and accelerates the liquid into the chamber. The fluid inertia parameter, I_f, that characterizes the intake fluid dynamics can be calculated from.

$$I_f = \frac{\rho L}{A} \tag{20}$$

where ρ is the liquid density, A is an appropriate area, and L is the intake pipe length.

Intake and Exhaust Area Modulation for the Two-Phase Flow Model

The intake and exhaust areas are funcitons of the scroll wrap geometry and orbit angle as in the single phase flow case, but the areas are also dependent on the quality of the fluid mixture at the intake and exhaust.

Quality, Q, in a thermodynamic sense, is defined as the mass of vapor, m_v, divided by the total mass, $m_T = m_v + m_L$, where m_L is the mass of the liquid, thus

$$Q = \frac{m_v}{m_v + m_L} \tag{21}$$

Eqn. (21) can be written in terms of fluid densities and volumes as,

$$Q = \frac{\rho_v V_v}{\rho_v V_v + \rho_L V_L} \tag{22}$$

or

$$Q = \frac{1}{1 + \frac{\rho_L V_L}{\rho_v V_v}} \tag{23}$$

The concept is that, as the orbiting scroll exposes the intake area, the area ratio between liquid and vapor is equal to the corresponding volume ratio. Thus,

$$\frac{A_L}{A_v} = \frac{V_L}{V_v} \tag{24}$$

Using eqn. (24) in (23) we can write,

$$\frac{A_L}{A_v} = \left(\frac{1}{Q} - 1\right)\frac{\rho_v}{\rho_L} = x \tag{25}$$

Then, since the total area, A_T, is

$$A_T = A_L + A_v \tag{26}$$

We can derive,

$$\frac{A_v}{A_T} = \left(\frac{1}{1 + x}\right) \tag{27}$$

and

$$\frac{A_L}{A_T} = \left(\frac{x}{1 + x}\right) \tag{28}$$

The total area is modulated as previously described by equations (12) and (13). Table 1 shows the calculated area ratios based on the fluid quality at the intake ranging from 1% to 99%, and the foregoing equations.

Heat Transfer Model

When the heat pump system is cool, a liquid/vapor mixture exists throughout the system and particularly at the compressor intake. The last section described how two-phase flow can be included in the model. Without heat transfer, the liquid phase of the flow would never vaporize and drive the mixture quality back to 100% vapor. Thus, it is important to include the fact that fluid compression will cause heat exchange between the fluid and machine case and some of this energy will vaporize the liquid phase of the mixture. To include this effect exactly is quite difficult, as the energy flow paths are both machine geometry and environment dependent. Here, we include heat transfer straightforwardly such that the heat transfer model parameters can ultimately be adjusted to match experimental observations.

The compressor heat transfer model accounts for the conductive energy flow from the fluid in the compression chamber to the case, and the thermal energy convected from the compressor case to the atmosphere. The liquid and vapor in the inlet pipe are assumed to be at saturated conditions, and the temperature of the intake pipe is assumed to be the case temperature. In addition, energy added to the inlet pipe all goes into heating the liquid and, subsequently, raises the enthalpy of the liquid in equilibrium with the vapor in the pipe. This in turn, drives liquid into its vapor phase thus varying the mixture quality. Fig. 9 shows the inlet pipe, with liquid and vapor, ready for ingestion into the compressor. The conductive and convective energy flows are indicated.

Fig. 10 shows the entire bond graph model of Fig. 3 only now including the heat transfer model. (Also, radial leakage is included in this complete representation.) A capacitance element, bond 119, accounts for the thermal energy stored in the case material. Variation in the case temperature, dT_c/dt, is determined by the relation

$$C\,\frac{dT_c}{dt} = Q_h \tag{29}$$

where the capacitance, C, is the product of the specific heat of the case material, C_c, and the case mass, m_c,

$$C = C_c m_c \tag{30}$$

Q_h is the sum of the energy flow from the compression chambers and the energy flow convected to the atmosphere. Rewriting eqn. (28) in terms of dT_c/dt and substituting eqn. (29) into eqn. (28) gives the state equation

$$\frac{dT_c}{dt} = \frac{Q_h}{C_c m_c} \tag{31}$$

Integrating (31) yields the case temperature as a function of time.

Thermal energy flow by conduction through a material of finite thickness, t, area, A_c, and thermal conductivity, k_c, may be written as

$$\dot{E}_{cond} = \frac{k_c A_c}{t}(T_{cham} - T_c) \tag{32}$$

Eqn. (32) is a resistance relationship for the pseudo-bond graph parts of Fig. 10. The resistance elements are represented by the one port R-elements on bonds 111,117, and 114 of Fig. 10. The total energy flow, Q_h, into the compressor case is the sum of the conductive energy flows from the individual chambers, bonds 112,115, and 118, and the energy convected to the atmosphere, bond 120.

Convective energy flow from the compressor case to the atmosphere is determined by,

$$\dot{E}_{conv} = h_c A_v (T_c - T_a) \tag{33}$$

where h_c is the thermal convection constant, A_v is an appropriate area, T_c is the case temperature, and T_a is atmospheric temperature. In this case, the thermal resistance is $1/(h_c A_v)$, on bond 122 of Fig. 10.

In this model, it is assumed that the inlet pipe temperature is the same as the case temperature, T_c. Energy flow from the pipe into the liquid is determined from

$$\dot{E}_{liq} = \frac{A_p k_c}{t_p}(T_c - T_i) \tag{34}$$

where A_p is the area of the pipe, k_c is the thermal conductivity of the case, t_p is the pipe thickness, T_c is the case temperature, and T_i is the intake liquid/vapor temperature.

Due to heat transfer from the case to the liquid, the quality of the fluid at the intake varies. Recall that the quality, Q, of a fluid mixture in a thermodynamic sense is

$$Q = \frac{M_{vap}}{M_{tot}} \tag{35}$$

where the total mass, M_{tot} is defined as the sum of the mass of the vapor, M_{vap}, and the mass of the liquid, M_{liq}.

$$M_{tot} = M_{vap} + M_{liq} \tag{36}$$

The change in the mass of the vapor is determined by the relation,

$$\frac{dM_{vap}}{dt} = \frac{\dot{E}_{liq}}{h_{l_v}} \tag{37}$$

where h_{lv} is the latent heat of vaporization for a saturated substance, and $\dot{E}_{liq}$ is the energy conducted to the liquid from the case, calculated from eqn. (34). Substituting eqn. (37) into eqn. (35) yields the change in the liquid quality as a function of the liquid energy flow and time,

$$\frac{dQ}{dt} = \frac{\dot{E}_{liq}}{M_{tot} h_{l_v}} \tag{38}$$

The quality, Q, is then used to set the inlet flow areas for the liquid and vapor as described previously.

In order to use the heat transfer model, an initial temperature for the case, and an initial quality of the fluid mixture at the compressor intake must be specified. Values for the conductive heat transfer and heat convection constants, the case surface area which is exposed to the atmosphere for conduction and convection, and the case thickness must also be specified in the program.

At each time interval during the simulation, the energy flows between the compressor chambers and the case are determined by eqn. (32) and the energy flow due to convection between the case and the atmosphere is determined by eqn. (33). Energy stored in the case due to its thermal capacitance increases the case temperature. The temperature difference between the liquid in the pipe and the case causes energy to flow between the pipe and the liquid. As previously mentioned, all of the energy is assumed to go into the liquid at the intake, and increases the enthalpy of the liquid in equilibrium with that of the vapor. The change in the quality of the liquid is calculated by eqn. (38). Eqn. (38) is integrated to yield the value of the quality as a function of time during the simulation. From the quality, the varying inlet areas for the liquid and vapor are calculated.

State Variables

For the single phase flow model, nine state equations are obtained from the model, three associated with each chamber. They are, for a chamber,

$$\dot{V} = \left(\frac{dV}{d\theta}\right)\left(\frac{d\theta}{dt}\right) \tag{39}$$

$$\dot{m}_{chamber} = \dot{m}_{intake} - \dot{m}_{exhaust} + \dot{m}_{flank\ leakage-in} - \dot{m}_{flank\ leakage-out} + \dot{m}_{radial\ leakage-in} - \dot{m}_{radial\ leakage-out} \tag{40}$$

$$\dot{E}_{chamber} = \dot{E}_{intake} - \dot{E}_{exhaust} + \dot{E}_{flank\ leakage-in} - \dot{E}_{flank\ leakage-out} - P\dot{V} + \dot{E}_{radial\ leakage-in} - \dot{E}_{radial\ leakage-out} \tag{41}$$

Two additional state equations are needed for each chamber for the two-phase flow model. These equations take into account the flow of incompressible fluid into and out of the chamber.

$$\dot{V}_{liquid} = \left(\frac{A}{\rho L}\right) P \tag{42}$$

where

$$\frac{dP}{dt} = (P_{atm} - P_{chamber}) \tag{43}$$

Also, as mentioned in the last section, the heat transfer model adds state equations like eqn. (38) for each chamber plus a state for the energy storage of the case.

Solution Technique

The Advanced Continuous Simulation Language (ACSL) [11] was used to simulate the compressor model. The model may be initialized at any desired orbit angle. The initial pressure and temperature must be specified for each chamber. The initial volume, mass, and energy are computed from the pressure and temperature specification. An integration time step of 0.001 seconds was used.

Simulation Results

The loss and leakage free case with area modulation and mass delay, the case with leakage, two-phase flow and heat transfer were all simulated using the three chamber bond graph model of Fig. 10. Scroll wrap dimensions are shown in Table 2. The orbit angle at which compression begins is 360 degrees, and the orbit angle at which discharge commences is 990 degrees.

Loss and Leakage Free Case: Atmospheric Conditions Exist at the Intake and Discharge Ports and Quality = 100%

The model was run for three complete cycles with the intake and exhaust port areas governed by eqns. (12) and 13). The compressor speed was set to 2800 RPM. Fluid at the intake was set to ambient conditions and, after completing the compression phase, the fluid was discharged into atmospheric conditions.

The volume as a function of the orbit angle is shown in Fig. 11. The pressure, as shown in Fig. 12, follows an isentropic path as expected. The temperature as a function of the orbit angle also follows an isentropic path until discharge. Mass flow into compression chamber 1 is shown in Fig. 13, and mass flow out of chamber 1 in Fig. 14.

Flank Leakage Case (Quality = 100%)

Flank leakage was incorporated into the program to investigate the effects on compressor performance. The ratio of fluid volume exhausted with leakage, to fluid volume exhausted without leakage, is plotted as a function of the clearance between the orbiting and stationary scroll in Fig. 15. The clearance may be thought of as the distance existing between the scroll wraps when they are assembled. If the distance between the wraps exceeds 1 micrometer, e.g., 0.1 millimeter, the gas volume exhaust ratio drops from 1 to .125.

Two-Phase Flow (Quality = 50%, and Quality = 1%)

The two-phase flow model was simulated for the quality of the fluid mixture at the intake equal to 50% and 1%. The compressor speed, RPM, was varied and the effects on the volume of liquid ingested by the compression chamber during the intake process evaluated. The volume of

liquid ingested by chamber 1 for a quality equal to 1% is plotted as a function of the compressor speed in Fig. 16. As the compressor speed is increased, the liquid volume ingested by the compression chamber decreases as shown, approaching zero at relatively high RPM's. High compressor speeds allow less time for accelerating the liquid, therefore, less fluid flows into the compression chamber as the speed increases. At 700 RPM, the volume of the liquid was 3.4E-6m^3. In comparison, the minimum volume of the compression chamber is 3.2E-6m^3, therefore, the minimum volume of the chamber was exceeded by the fluid volume. This did not occur at the other specified compressor speeds so that a volume was available for receiving and compressing the gas.

The discharge pressure and temperature in the chamber with the liquid volume resident in the machine is higher than the discharge pressure as shown in Fig. 12 and temperature for the loss and leakage free case. The volume of liquid occupying the chamber reduces the compression chamber volume available to compress the gas, thus the chamber pressure and temperature increase.

As the quality of the intake fluid was increased, the volume of liquid ingested by the compression chamber decreased significantly. Since the volume flow of liquid into the compression chamber is proportional to the liquid intake area, as governed by eqn. (42), a reduction or increase in the liquid intake area, due to a respective increase or decrease in the quality, results in a reduction or rise in the flow of fluid, accordingly. The liquid volume ingested by chamber 1 as a function of compressor speed for a quality equal to 50% is shown in Fig. 17. The maximum volume of liquid ingested by the compression chamber at a compressor speed of 700 RPM is 3.28-8m^3. This is much smaller than the minimum volume of the compression chamber, based on the dimensions outlined in Table 2, by a factor of approximately 100.

Heat Transfer and Two-Phase Flow

The complete model of Fig. 10 was simulated for the case of no leakage, but including heat transfer and two-phase flow. The initial intake fluid quality was set to 95%. The thermal resistance for conduction and convection were chosen to yield a three minute time constant.

Chamber pressure and temperature time histories (not shown) exhibited reduced peak values since the heat energy, which would otherwise be resident in the chamber, is extracted from the machine.

All of the thermal energy conducted into the intake pipe from the machine is assumed to go into heating the liquid at the intake. The intake quality, as seen in Fig. 18, increases as the thermal energy converts the liquid into vapor. As the quality increases, the liquid flow area decreases, and the liquid ingested decreases as seen in Fig. 19.

Conclusions

A model was developed for a three chamber scroll compressor using the bond graph modeling procedure. Bond graphs allow the mechanical and thermodynamic interactions of the machine to be coupled in a unified manner. Through causality, bond graphs also insure that a computable model results, and permit straightforward derivation of state equations. The model includes leakage between scroll chambers, two-phase flow at the intake, and heat transfer.

The model developed here has not been compared to experimental data at this time. However, the purpose of this paper is to demonstrate the modeling procedure and its applicability to rotating machines. The outputs appear reasonable, and the model can currently be used to predict expected performance deviations from a benchmark case, for changes in machine parameters such as size, mass, RPM, inlet conditions, etc. Our plan is to use the compressor model in an overall model of a heat pump system.

References

[1] Margolis, D.L., "Analytical Modeling of Helical Screw Turbines for Performance Prediction," ASME Journal of Engineering for Power, Vol. 100, July 1978, pp. 482-487.

[2] Merala, Raymond, et. al, "Modeling and Simulation of a Supercharger," ASME Journal of Dynamic Systems, Measurement, and Controls, Vol. 110, September 1988, pp. 316-323.

[3] Welch, Mark S., "Modeling and Simulation fo a General Wankel Compressor," M.S. thesis, University of California, Davis, 1988.

[4] Morishita, Etsuo, et. al, "Scroll Compressor Analytical Model," 1984 Purdue Compressor Technology Conference, pp. 487-495.

[5] Tojo, K. et. al, "Computer Modeling of Scroll Compressor with Self Adjusting Back-Pressure Mechanism," 1986 Purdue Compressor Technology Conference, pp. 872-886.

[6] Nieter, J., et. al, Dynamics of Scroll Suction Process," 1988 Purdue Compressor Technology Conference, pp. 165-174.

[7] Hayano, M. et. al, "An Analysis of Losses in Scroll Compressor," 1988 Purdue Compressor Technology Conference, pp. 189-197.

[8] Karnopp, D., Margolis, D. and Rosenberg, R., *System Dynamics: A Unified Approach*, Wiley, New York, 1990.

[9] Rosenberg, R. and Karnopp, D., *Introduction to Physical System Dynamics*, McGraw Hill Book Company, New York, 1983.

[10] Karnopp, D., "State Variables and Pseudo Bond Graphs for Compressible Thermofluid Systems," ASME Journal of Dynamic Systems, Measurement and Controls, Vol. 101, No. 3, Sept. 1979, pp. 201-204.

[11] Mitchell and Gauthier Associates, Concord, Mass. 01742, Advanced Continuous simulation Language Reference Manual, 1986.

[12] Beseler, Frederick, "Scroll Compressor Technology Comes of Age," Heating/Piping/Air Conditioning, July 1987, pp. 67-70.

QUAL GAS	QUAL LIQ	ALIQUATOTAL	AVAPATOTAL
0.99	0.01	1.2148E-05	0.999987851
0.95	0.05	6.32845-05	0.99993672
0.9	0.1	0.0001336	0.9998664
0.85	0.15	0.00021219	0.99978781
0.8	0.2	0.0003006	0.9996994
0.75	0.25	0.00040081	0.9995992
0.7	0.3	0.00051532	0.99948468
0.65	0.35	0.00064745	0.99935255
0.6	0.4	0.0008019	0.9991981
0.55	0.45	0.00098379	0.99901621
0.5	0.5	0.0012024	0.9987976
0.45	0.55	0.00146961	0.99853039
0.4	0.6	0.00180361	0.99819639
0.35	0.65	0.00223304	0.99776696
0.3	0.7	0.00280561	0.99719439
0.25	0.75	0.00360721	0.99639279
0.2	0.8	0.00480962	0.99519038
0.15	0.85	0.00681363	0.99318637
0.1	0.9	0.01082154	0.98917846
0.05	0.95	0.02284569	0.97715431
0.01	0.99	0.11903805	0.88096192

Table 1 Area ratios as a function of the quality of the fluid at the inlets

Height, h	37.6E-3m
Thickness, t	4.5E-3m
Base circle radius, a	2.6E-3m
Pitch, P	16.3E-3m
Crank arm radius, ζ	4.5E-3m

Table 2. Scroll wrap dimensions used in the simulations.

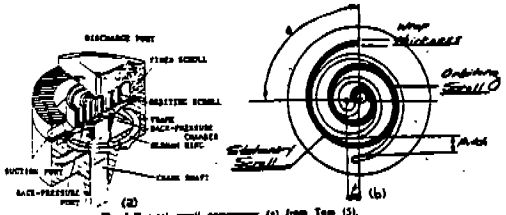

Fig. 1 Typical scroll compressor (a) from Tojo [5].
Scroll wrap dimensional parameters (b).

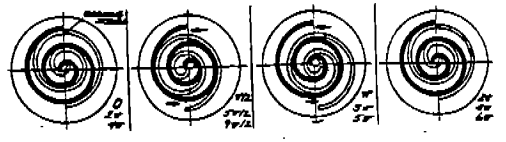

Fig. 2 Compression ... Proto [12]

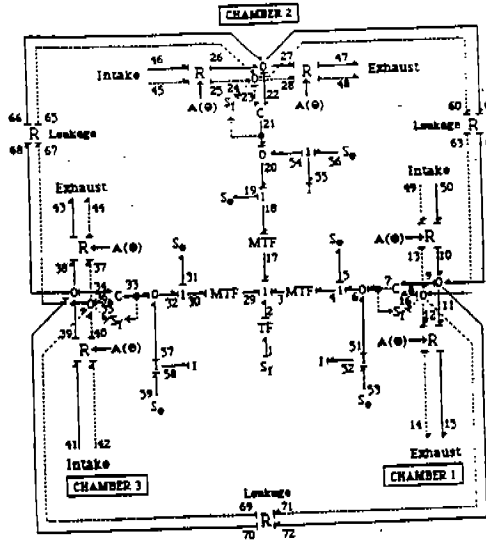

Fig. 3 Bond graph for the three chamber scroll compressor with flank leakage and two-phase flow

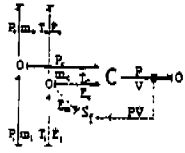

Fig. 4 Bond graph element: thermodynamic accumulator

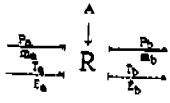

Fig. 5 Bond graph element: Isentropic Nozzle

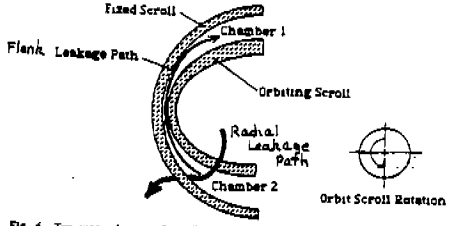

Fig. 6 Top view of a set of scroll wraps showing flank leakage path between chamber 1, and chamber 2 during the first 720 degrees of the compression cycle.

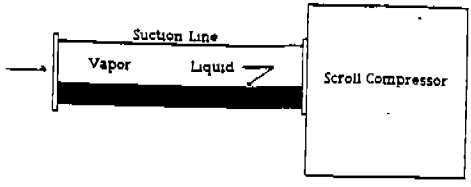

Fig. 7 Schematic of the two-phase flow model.

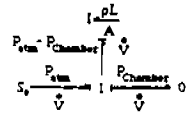

Fig. 8 Inertia element used to simulate the liquid flow modal shown in Fig. 6.

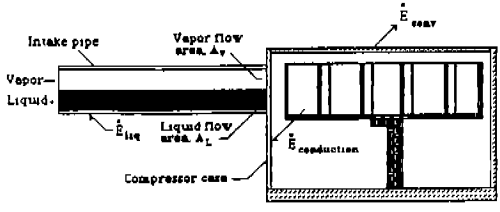

Fig. 9 Compressor thermal model with energy flows calculated in the simulation

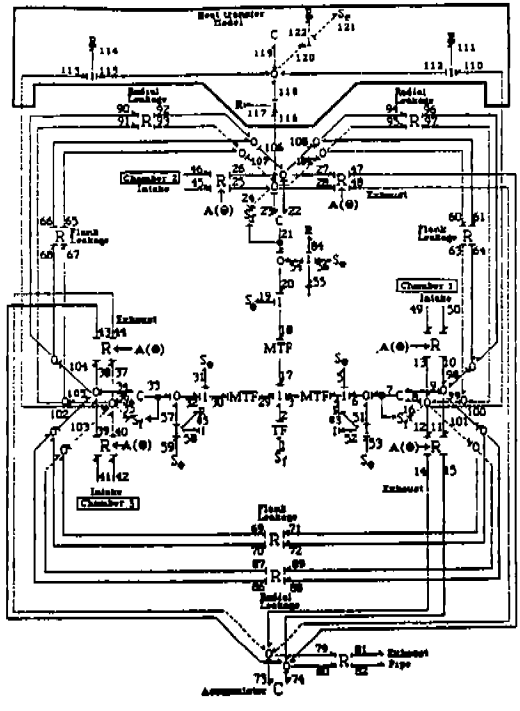

Fig. 10 Overall scroll compressor bond graph

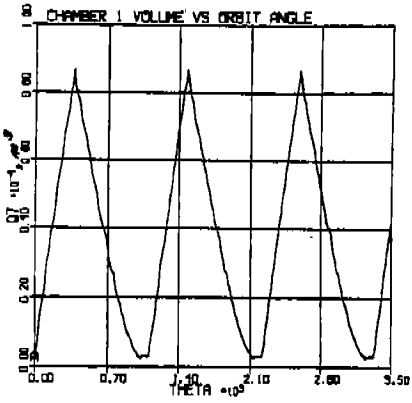

Figure 11

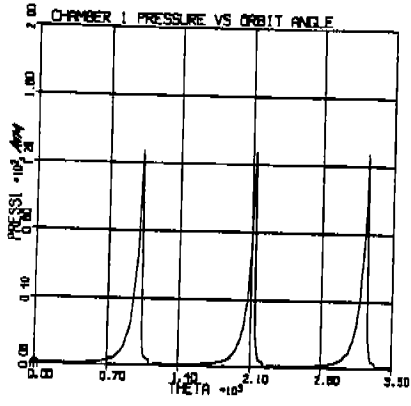

Figure 12

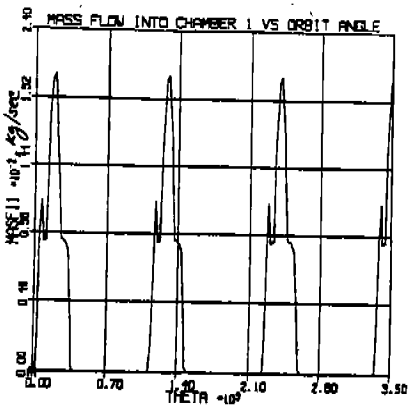

Figure 13

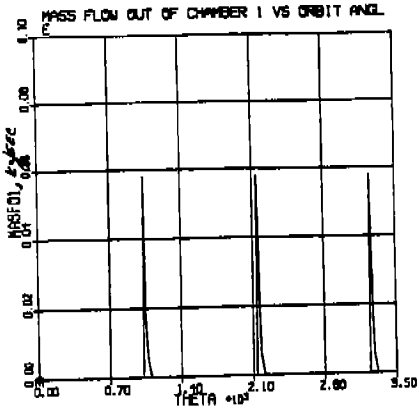

Figure 14

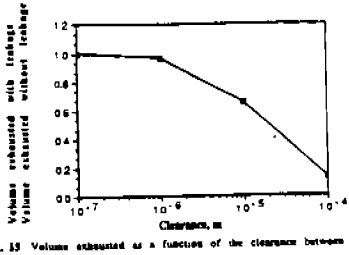

Fig. 15 Volume exhausted as a function of the clearance between the stationary and orbiting wrap.

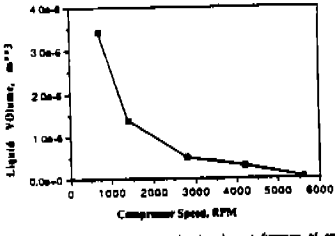

Fig. 16 Liquid volume ingested by chamber 1 as a function of compressor speed for a fluid intake quality equal to 1%.

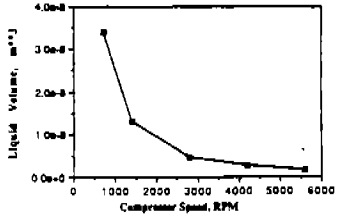

Fig. 17 Volume of liquid ingested by chamber 1 as a function of compressor speed for fluid quality equal to 50%.

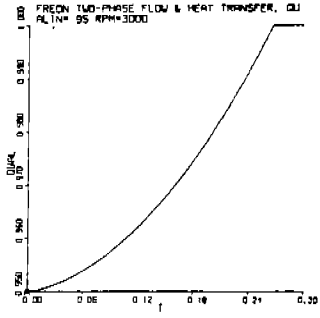

Figure 18. Intake fluid quality as a function of time. Two-phase flow and heat transfer case.

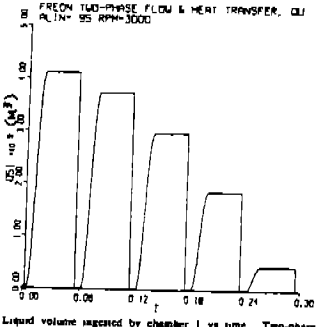

Figure 19. Liquid volume ingested by chamber 1 vs time. Two-phase flow and heat transfer case.